Directional Sensitivity In Light-Mass Dark Matter Searches With Single-Electron Resolution Ionization Detectors

Fedja Kadribasic, Nader Mirabolfathi
Department of Physics and Astronomy, Texas A&M University

Kai Nordlund, Eero Holmström, Flyura Djurabekova
Helsinki Institute of Physics and Department of Physics, University of Helsinki

(Dated: March 22, 2017)

We present a method for using solid state detectors with directional sensitivity to dark matter interactions to detect low-mass Weakly Interacting Massive Particles (WIMPs) originating from galactic sources. In spite of a large body of literature for high-mass WIMP detectors with directional sensitivity, there is no available technique to cover WIMPs in the mass range <1 GeV/c^2. We argue that single-electron resolution semiconductor detectors allow for directional sensitivity once properly calibrated. We examine commonly used semiconductor material response to these low-mass WIMP interactions.

arXiv:1703.05371v2 [physics.ins-det] 20 Mar 2017

A large body of astrophysical observations indicate that 85% of the matter in the universe is not made of recognized standard model particles [1]. Understanding the nature of this dark matter is of fundamental importance to cosmology, astrophysics, and high energy particle physics. Although Weakly Interacting Massive Particles (WIMPs) of mass 10-100 GeV/c^2 have been the main interest of the majority of direct dark matter detection experiments, recent signal claims, alongside compelling theoretical models, are shifting the old paradigm to include broader regions in the dark matter parameter space well below 10 GeV/c^2[2].

Direct detection experiments attempt to detect WIMPs via their elastic interaction with detector nuclei [3]. Since very low energy nuclear recoils and small interaction rates from these low-mass WIMPs are expected, large-mass detectors with very low threshold are desirable. Solid state detectors, in particular those utilizing phonon-mediated readout technology, have already achieved or are braced to reach the sensitivities required to detect these very-low-mass WIMPs [4].

The sensitivity of WIMP direct search experiments is subject to both reducible (environmental) and irreducible (solar neutrino) backgrounds that may mimic WIMPs. A potential tool to circumvent these backgrounds is the directionality of the WIMPs' signal due to Earth's motion through their isothermal halo distribution in our galaxy. The WIMP velocity distribution in the lab frame, and hence the expected direction of the WIMP-induced recoils, varies daily depending on the angular orientation of the detectors with respect to the galactic WIMP flux.

Although many experiments are proposing to track WIMP-induced recoils using low-pressure gas or even liquid scintillators, they do not offer energy thresholds low enough to detect recoils induced from low-mass WIMP interactions (<1 GeV/c^2) [5]. Furthermore, for the case of low-pressure-gas detectors, prohibitively large volume detectors are required to detect any noticeable WIMP signal. We argue that single-electron resolution phonon-mediated semiconductor detectors such as those in development for SuperCDMS and future generation-3 dark matter experiments are sensitive to the nuclear recoil direction and can be used for a directional dark matter search.

Our method utilizes the fundamental processes involved in nuclear recoil ionization excitation whose threshold exhibits a strong recoil direction dependence. Phonon-mediated detectors, in particular those using the Neganov-Luke phonon amplification effect to measure ionization in semiconductor detectors [6], are the most appropriate to detect this anisotropy effect. Recent progress utilizing this technology gives hope for future large-mass semiconductor detectors with single-electron resolution [7].

There is neither a computational framework nor experimental data to estimate the minimum energy required to create single electron-hole pair excitations via nuclear recoil interactions. We make a reasonable assumption that this threshold is equal or proportional to the minimum energy required to displace the recoiling nucleus and create a defect in the crystal. This is in contrast to the current standard nuclear recoil ionization yield estimates that are based on the extension of the Lindhard model [8, 9] down to the single pair excitation threshold. In that model, the incident particle ejects the recoiled atom from the lattice with the ionization yield proportional to recoil velocity. The model should fail for very low recoil velocities wherein the ejected atom has no energy left to create further quantum excitations [10–13]. We are assuming that at these low energies the sudden creation of lattice defects provides enough local perturbation in the electronic band structure to create an electron-hole pair excitation. Below, we demonstrate that the threshold for this lattice defect creation process is a strong function of recoil angle.

We consider the threshold variation for two common detector materials, Ge and Si. For both, density-functional theory (DFT) molecular dynamics simulations

have previously been used to obtain the average threshold displacement energy, as well as the direction-specific values in the ⟨100⟩ and ⟨111⟩ crystal directions [14, 15]. However, to obtain a smooth description of the threshold displacement energy surface by utilizing this method is practically impossible due to the high computational cost of DFT. Instead, we used molecular dynamics simulations [16] with computationally more efficient classical interatomic potentials, following the procedure described in Ref. [17].

Put succinctly, a 4096 atom Ge or Si simulation cell was equilibrated at 0.04 K (an upper limit for the experimental detector temperature); an atom was randomly chosen within the central eight unit cells of the simulation cell, and given a recoil of energy E in a randomly selected direction (θ, ϕ) in three dimensions (θ is defined as the polar angle off the [001] crystal direction, and ϕ as the azimuthal angle from the [100] direction towards [010]). The evolution of the collision sequence thus generated was simulated for 10 ps, and possible defect creation was analyzed automatically using Wigner-Seitz and potential energy criteria [17]. For each atom and direction, the energy E was increased starting from 2 eV in steps of 1 eV until a stable defect was created.

The outcome of molecular dynamics simulations depends crucially on the interatomic potential used [16, 17]. Hence, for the purpose of this study, we tested several different Ge and Si interatomic potentials against the DFT results. Among the three tested interatomic potentials for Ge [18–20], the modified Stillinger-Weber potential from Ref. [19] reproduced all of the reported DFT threshold displacement energies [15] within the error bars, giving us high confidence of a reliable description of the entire data range. Hence, this potential was used for all Ge simulations.

We have previously shown that, out of three commonly used Si potentials, the Stillinger-Weber one [21] is able to reproduce the DFT and experimental results the closest. We use this potential to calculate the rates in Si.

In total, about 85,000 directions for Ge and about 24,000 for Si were simulated a total of eight times. The average over the resulting threshold displacement energy surfaces is illustrated for Ge and Si in Fig. 1. The data is periodic with respect to $\phi = 45°$ because of the symmetry of the diamond crystal structure.

Fig. 1 shows that the energy threshold to create a defect strongly depends on the nuclear recoil direction. Even for the average threshold energies, there is a variation of more than a factor of two in the value of the threshold. Additionally, the overall threshold is larger for Si than for Ge.

The expected total WIMP signal rate above the detection threshold can be calculated by integrating the differential rate over the recoil angle and recoil energy. In the case of a charge detector, the energy thresholds, henceforth referred to as $E_{th}(\theta, \phi)$ and shown in Fig. 1,

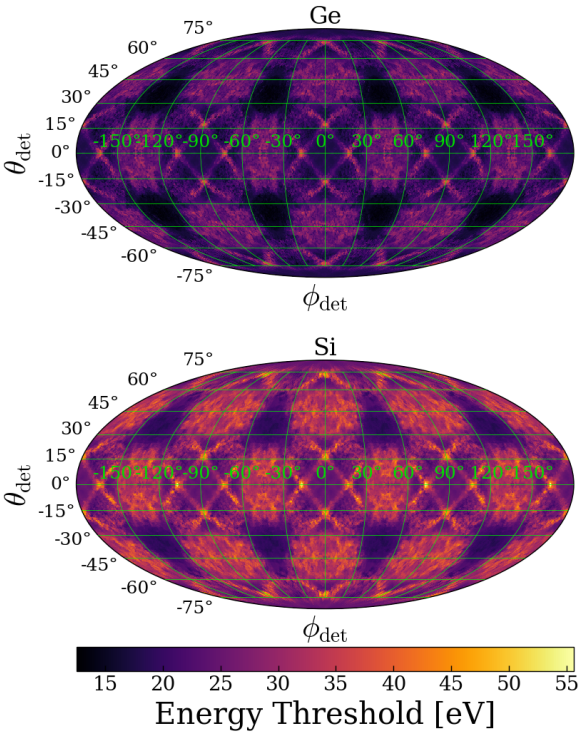

FIG. 1. Threshold displacement energy surface in different crystal directions in Ge (top) and Si (bottom) determined from classical molecular dynamics simulations illustrated with a Mollweide projection. These plots represent the averages over the eight threshold surface datasets. There is large variation in displacement threshold energy over recoil angle, and the overall threshold is larger for Si than for Ge.

simply provide the lower limit to the integral

$$R(t) = \oint_{4\pi} \int_{E_{th}(\theta,\phi)}^{E_r^{max}} \frac{\partial^2 R}{\partial E_r \partial \Omega_r} \mathrm{d}E_r \mathrm{d}\Omega_r. \qquad (1)$$

This rate measured by a fixed detector on the surface of Earth, which is moving and rotating relative to the WIMP halo, should therefore exhibit a diurnal modulation since E_{th} is a function of θ and ϕ. Below we describe our procedure to calculate this integral.

Based on the calculations in [22], the differential interaction rate, the integrand in Eq. 1, between halo WIMPs and detectors for spin-independent interactions, is

$$\frac{\partial^2 R}{\partial E_r \partial \Omega_r} = \frac{\rho_0 \sigma A^2}{4\pi m_\chi \mu_{\chi n}^2} \times F^2(E_r) \hat{f}_{\rm lab}(v_{\rm min}, \hat{\boldsymbol{q}}_{\boldsymbol{r}}; t) \qquad (2)$$

where m_χ is the WIMP mass, $\mu_{\chi n}$ is the WIMP-nucleon reduced mass, $\rho_0 = 0.3$ GeV cm^{-3} is the local dark matter density, A is the mass number of the nucleus, σ is the WIMP-nucleon cross section, $v_{\rm min} = \sqrt{2 m_N E_r}/2\mu_{\chi n}$ is the minimum WIMP speed required to produce a nu-

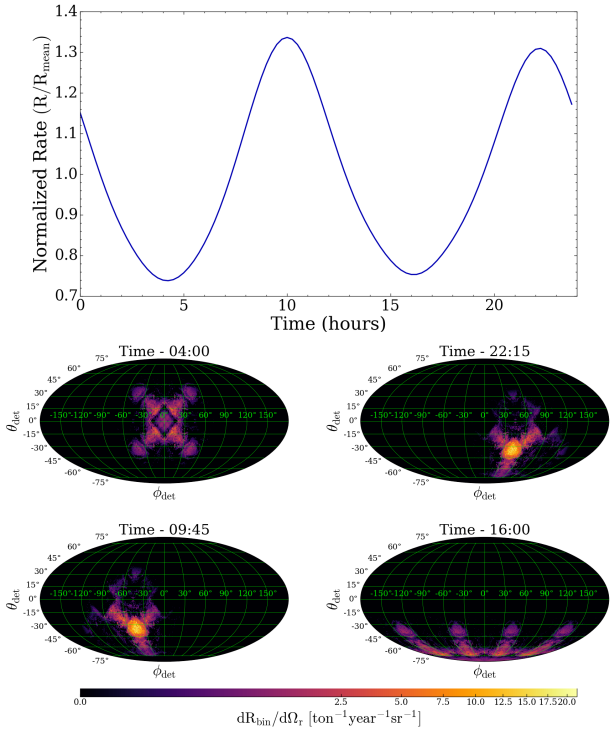

FIG. 2. (Top) Normalized integrated signal rate with respect to mean over one day for a 300 MeV/c^2 WIMP at the SNOLAB site. (Bottom) Angular distribution of $\partial R/\partial\Omega_r$ for a nucleon cross section of 10^{-39}cm^2 over one day for a 300 MeV/c^2 WIMP at the SNOLAB site. Each of the four times corresponds to a local extremum of the integrated rate.

clear recoil of energy E_r for a given nuclear mass m_N, and $F^2(E_r)$ is the Helm nuclear form factor [23].

The Radon transform of the WIMP velocity distribution $f_{\rm lab}(\boldsymbol{v})$ is given by

$$\hat{f}_{\rm lab}(v_{\rm min},\hat{\boldsymbol{q}};t) = \frac{1}{N_{\rm esc}\sqrt{2\pi\sigma_v^2}}\times \left[\exp\left(-\frac{|v_{\rm min}+\hat{\boldsymbol{q}}\cdot\boldsymbol{v}_{\rm lab}|^2}{2\sigma_v^2}\right)-\exp\left(-\frac{v_{\rm esc}^2}{2\sigma_v^2}\right)\right] \quad (3)$$

where $\hat{\boldsymbol{q}}$ is the recoil direction in detector coordinates, $\boldsymbol{v}_{\rm lab}$ is the velocity of the laboratory relative to a stationary observer, $v_{\rm esc}$ is the escape velocity at the Solar System's distance from the Milky Way's center, $\sigma_v = v_0/\sqrt{(2)}$ is the dark matter velocity dispersion, and $N_{\rm esc}$ is a normalization factor. We use $v_0 = 220$ km s^{-1} for the circular speed and $v_{\rm esc} = 544$ km s^{-1} [22].

Following the procedure set out in Appendix B of [24], we calculate the total lab velocity using the contributions due to galactic rotation, solar motion, Earth's revolution, and Earth's rotation. The detector for this analysis is assumed to be at SNOLAB, whose coordinates are $(46.4719°, 81.1868°)$. The variation in lab-frame speed of the dark matter gives a ∼6% annual and nearly negligible diurnal modulation [25].

We calculate signal rates assuming a detector with 1 eV resolution, 100% detection efficiency, and no backgrounds. We perform the integral in Eq. 1 over the recoil energy E_r, with the lower limit set by Fig. 1, and recoil angle Ω_r using 48 time steps on September 6, 2015. The date was chosen in order to cross-check our differential rate calculations with those in [22]. An equidistant coordinate partition interpolation of the data shown in Fig. 1 is performed on a grid with 2400 elements in the θ direction and 4800 in the ϕ direction. For faster computation, the grid is resampled to a size of 196,608 pixels using the HEALPix algorithm [26]. We compute a multidimensional Riemann sum over each dimension with 200 sample points for E_r and 196,608 for Ω_r.

Fig. 2 shows the integrated event rate for a WIMP of mass 300 MeV/c^2 and cross section σ=10^{-39}cm^2 over the course of one day (Sept 6th 2015). The mass and cross section were arbitrarily chosen within the unexplored region in the halo WIMP parameter space. Also shown in this figure are the angular distribution of the rates at four different times illustrating recoil orientation change with respect to the crystal over the course of the day. As Earth rotates, the energy threshold is effectively sampling regions close to the energy threshold minima more than those near the maxima leading to an integrated rate modulation (in this case ∼60%) with a phase that is imposed by the threshold data in Fig. 1.

We repeated this study for WIMPs covering a range of mass between 230 MeV/c^2 and 10 GeV/c^2 for Ge and between 165 MeV/c^2 and 10 GeV/c^2 for Si. In our model, lower-mass WIMPs do not produce stable defects or electron-hole pair excitation even when traveling at the escape velocity $v_{\rm esc} = 544$ km s^{-1}. Fig. 3 shows the recoil angular distribution in Ge at a given time (4:00 on September 6, 2015) for a sample of WIMP masses in this range. As shown in this figure, larger mass WIMPs produce a broader recoil angle distribution. Hence, the integrated signal rate associated with larger mass WIMPs is less sensitive to the crystallographic orientation of the detector. We expect smaller event rate modulation for larger mass WIMPs due to this effect.

To assess the strength of the signal rate modulation with respect to the signal mean rate we perform a normalized RMS integral over one day,

$$R_{\rm RMS,\ norm} = \sqrt{\frac{1}{\langle R\rangle^2\Delta t}\oint_{\Delta t}(R(t)-\langle R\rangle)^2 dt} \quad (4)$$

where $\langle R\rangle$ is the average value over Δt, which is one solar day (24 hours). The results of these studies are shown in Fig. 4. We find a clear rate modulation for WIMPs of mass below 1 GeV/c^2. As expected, while the signal mean rate (thicker graph) decreases for lower mass WIMPs, the modulation gains strength. This increased modulation strength at lower WIMP masses enables the experiments to maintain their signal to background ratio

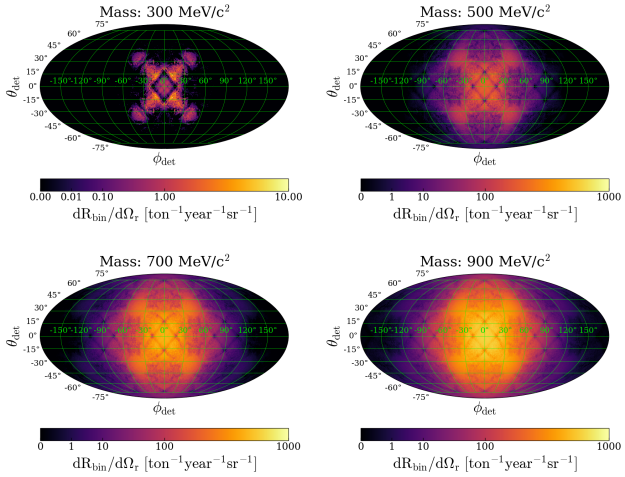

FIG. 3. Angular distribution of $\partial R/\partial\Omega_r$ for a Ge detector assuming a nucleon cross section of 10^{-39}cm^2 for several WIMP masses at 4:00 on September 6, 2015. As the WIMP mass increases, the differential rate angular spread increases due to the Maxwell-Boltzmann velocity distribution and hard-sphere scattering acting in conjunction with the energy thresholds.

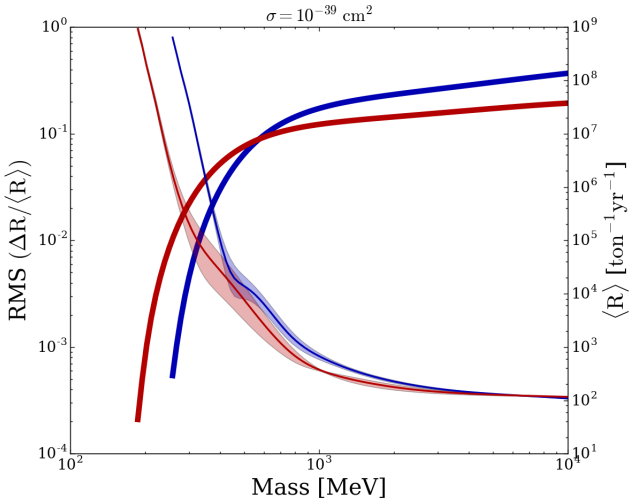

FIG. 4. Normalized root mean square of the rate modulation (left axis, thin lines) and mean rate (right axis, thick lines) as a function of WIMP mass for Ge (blue) and Si (red). We assume a WIMP-nucleon cross section of 10^{-39}cm^2. RMS error is given by the shaded regions. Mean rate error is negligible and consequently not included.

by only looking at the intervals of time wherein the signal rate is expected to be maximum. Furthermore, since the Si nucleus is less massive than that of Ge, the energy transfer from a WIMP is more efficient, and hence a lower WIMP mass is required to give a recoil energy sufficient to overcome the threshold displacement energy. Consequently, the peak of the modulation appears at lower WIMP masses for Si than for Ge.

The Stillinger-Weber potential that was used in this report to produce Si threshold data in Fig. 1 overestimates the minimum threshold energy in the $\langle 111\rangle$ direction [27]. We expect the modulation to peak at lower WIMP masses for Si than those found in this paper when this experiment is carried out. This could also result in a higher modulation overall for Si.

The threshold displacement energy is highly stochastic due to the atoms interacting with strongly coupled many-body interactions, leading to a chaotic system where even the very small thermal vibrations can lead to major changes in the outcome of individual events. As noted previously, we calculate eight separate threshold datasets for Ge and Si using molecular dynamics simulations. The mean and standard deviation of the RMS values over all eight are plotted as the RMS curves and shaded regions in Fig. 4.

The bump-like features in these data are due to the transition between small and large recoil solid angle coverage. As shown in Fig. 3, the larger the solid angle, the more threshold minima and maxima are included. This also explains the larger error bars at these transition points since a small deviation in the threshold results in a large change in the modulation amplitude.

In conclusion, based on the substantiated observation that the threshold energy for defect creation depends on crystal direction, we demonstrated a strong diurnal modulation in the expected halo WIMP detection rate for WIMPs below 1 GeV/c^2. Furthermore, this modulation strongly depends on the target detector material and WIMP mass, and, together with the overall mean rate, it provides an extra handle to determine WIMP mass and cross section independently. This effect can also be used to discriminate WIMPs from solar neutrino backgrounds which would become the irreducible background for all dark matter search experiments. In a follow-up paper, we will demonstrate the sensitivity reach for this method in the presence of the solar neutrino and other experimental backgrounds. Future low-mass WIMP search experiments are about to deploy detectors with sufficiently low thresholds to be sensitive to this daily rate modulation. The significance of these results motivates a thorough calibration of semiconductor material at such low recoil energies and their crystallographic orientation dependencies.

N.M. acknowledges financial support from Mitchell Institute for Fundamental Physics and Astronomy at Texas A & M University. N. M. and F. K. are very thankful for helpful discussions and feedback from Louis Strigari and Rupak Mahapatra. E. H. acknowledges financial support from the Emil Aaltonen foundation and the Academy of Finland through the Centres of Excellence Program (Project No. 251748).

[1] P. A. R. Ade *et al.* (Planck), Astron. Astrophys. **571**, A16 (2014), arXiv:1303.5076 [astro-ph.CO].

[2] P. Cushman *et al.*, *Proceedings, 2013 Community Summer Study on the Future of U.S. Particle Physics: Snowmass on the Mississippi (CSS2013): Minneapolis, MN, USA, July 29-August 6, 2013*, (2013), arXiv:1310.8327 [hep-ex].

[3] R. J. Gaitskell, Ann. Rev. Nucl. Part. Sci. **54**, 315 (2004).

[4] R. Agnese *et al.* (SuperCDMS), Phys. Rev. Lett. **112**, 041302 (2014), arXiv:1309.3259 [physics.ins-det].

[5] F. Mayet *et al.*, Phys. Rept. **627**, 1 (2016), arXiv:1602.03781 [astro-ph.CO].

[6] P. N. Luke, J. Beeman, F. S. Goulding, S. E. Labov, and E. H. Silver, *Nucl. Instrum. Methods A289 (1990) 406-409.*, Nucl. Instrum. Meth. **A289**, 406 (1990).

[7] N. Mirabolfathi, H. R. Harris, R. Mahapatra, K. Sundqvist, A. Jastram, B. Serfass, D. Faiez, and B. Sadoulet, Nucl. Instrum. Meth. **A855**, 88 (2017), arXiv:1510.00999 [physics.ins-det].

[8] J. Lindhard, V. Nielsen, M. Scharff, and P. Thomsen, Kgl. Danske Videnskab., Selskab. Mat. Fys. Medd. **Vol: 33: No. 10** (1963).

[9] J. D. Lewin and P. F. Smith, Astropart. Phys. **6**, 87 (1996).

[10] J. E. Valdes, C. Parra, J. Diaz-Valdes, C. D. Denton, C. Agurto, F. Ortega, N. R. Arista, and P. Vargas, Phys. Rev. A **68**, 064901 (2003).

[11] S. N. Markin, D. Primetzhofer, and P. Bauer, Physical Review Letters **103**, 113201 (2009).

[12] D. Primetzhofer, Phys. Rev. B **86**, 094102 (2012).

[13] A. Lim, W. M. C. Foulkes, A. P. Horsfield, D. R. Mason, A. Schleife, E. W. Draeger, and A. A. Correa, Phys. Rev. Lett. **116**, 043201 (2016).

[14] E. Holmström, A. Kuronen, and K. Nordlund, Phys. Rev. B **78**, 045202 (2008).

[15] E. Holmstrm, K. Nordlund, and A. Kuronen, Physica Scripta **81**, 035601 (2010).

[16] M. P. Allen and D. J. Tildesley, *Computer Simulation of Liquids* (Oxford University Press, Oxford, England, 1989).

[17] K. Nordlund, J. Wallenius, and L. Malerba, Nucl. Instr. Meth. Phys. Res. B **246**, 322 (2005).

[18] K. Ding and H. C. Andersen, Phys. Rev. B **34**, 6987 (1986).

[19] K. Nordlund, M. Ghaly, R. S. Averback, M. Caturla, T. Diaz de la Rubia, and J. Tarus, Phys. Rev. B **57**, 7556 (1998).

[20] M. Posselt and A. Gabriel, Phys. Rev. B **80**, 045202 (2009).

[21] F. H. Stillinger and T. A. Weber, Phys. Rev. B **31**, 5262 (1985).

[22] C. A. J. O'Hare, A. M. Green, J. Billard, E. Figueroa-Feliciano, and L. E. Strigari, Phys. Rev. **D92**, 063518 (2015), arXiv:1505.08061 [astro-ph.CO].

[23] G. Duda, A. Kemper, and P. Gondolo, JCAP **0704**, 012 (2007), arXiv:hep-ph/0608035 [hep-ph].

[24] N. Bozorgnia, G. B. Gelmini, and P. Gondolo, Phys. Rev. **D84**, 023516 (2011), arXiv:1101.2876 [astro-ph.CO].

[25] The annual modulation is mostly due to Earth's revolution around the sun, whereas the daily one is due to Earth's rotation.

[26] K. M. Gorski, E. Hivon, A. J. Banday, B. D. Wandelt, F. K. Hansen, M. Reinecke, and M. Bartelman, Astrophys. J. **622**, 759 (2005), arXiv:astro-ph/0409513 [astro-ph].

[27] E. Holmström, A. V. Krasheninnikov, and K. Nordlund, in *Ion Beams and Nano-Engineering*, MRS Symposium Proceedings, Vol. 1181, edited by D. Ila, J. K. N. Lindner, P. K. Chu, J. Baglin, and N. Kishimoto (MRS, Warrendale, PA, USA, 2010) pp. 111–122.